

## Homonuclear Two-Dimensional $^1\text{H}$ NMR of Proteins. Experimental Procedures

G. WIDER,<sup>\*,&</sup> S. MACURA,<sup>\*,+,\\$</sup> ANIL KUMAR,<sup>\*,+,\\$</sup> R. R. ERNST,<sup>+</sup>  
AND K. WÜTHRICH<sup>\*</sup>

<sup>\*</sup>*Institut für Molekularbiologie und Biophysik, and <sup>+</sup>Laboratorium für Physikalische Chemie,  
Eidgenössische Technische Hochschule, CH-8093 Zurich, Switzerland*

Received May 9, 1983; revised July 26, 1983

Experimental techniques used for homonuclear 2D  $^1\text{H}$  NMR studies of proteins are described. A brief survey of the general strategy for structural studies of proteins by 2D NMR is included. The main part of the paper discusses guidelines for the selection of experimental techniques, the elimination of artifacts and unwanted peaks in protein 2D  $^1\text{H}$  NMR spectra, suppression of the solvent line in  $\text{H}_2\text{O}$  solutions, experimental parameters, numerical data processing before and after Fourier transformation, and suitable presentations of complex 2D NMR spectra.

### I. INTRODUCTION

During the past five years it was demonstrated that well-resolved, informative two-dimensional (2D)  $^1\text{H}$  NMR spectra of proteins in solution can be recorded with commercially available high-resolution NMR equipment (1-5). The fundamental experimental schemes of the experiments which have most profitably been used for studies of proteins are shown in Fig. 1 (1-3, 6-10). With the use of 2D NMR nearly complete individual proton resonance assignments have been obtained for several small proteins (11-19) and 2D NMR investigations of static and dynamic aspects of the conformations of these proteins in solution are in progress (e.g., 20-24). With the exception of some reports on conceptually new procedures (8, 25-33), our earlier publications contain little information on experimental details of the 2D NMR measurements. The present paper describes salient points from our practical experience gained when optimizing the experimental conditions for homonuclear 2D  $^1\text{H}$  NMR with proteins.

While the scope of the present article is limited to technical aspects which have been of particular relevance for homonuclear  $^1\text{H}$  experiments with proteins, much of this information should be of interest also for studies of other classes of large molecules. Several reviews are already available which survey the procedures used for the study of low molecular weight compounds (e.g., 34-36).

& Present address: Spectrospin AG, Industriestrasse 26, CH-8117 Fällanden, Switzerland.

\\$ Present address: Institute of Physical Chemistry, Faculty of Science, 1100 Beograd, Yugoslavia.

\\$ Present address: Department of Physics, Indian Institute of Science, Bangalore, India.

## II. STUDIES OF PROTEIN STRUCTURE AND CONFORMATION BY 2D NMR

This section presents a brief discussion of a 2D NMR strategy used for the elucidation of protein conformation. Three basic types of 2D experiments have proved valuable in this context (Fig. 1):

(A) 2D NOE spectroscopy (NOESY) (10, 3) delivers maps which demonstrate spatial proximity of nuclei based on their mutual cross-relaxation producing magnetization transfer manifested in nuclear Overhauser effects (NOE). The experiment requires an extensive mixing period separated from evolution and detection periods by two  $\pi/2$  pulses (Figs. 1A and A').

(B) 2D correlated spectroscopy (COSY) (7, 2, 9) produces correlation maps which display the connectivity of nuclei by spin-spin coupling. A COSY spectrum thus provides information on proximity of nuclei along the chemical bonds. The correlation is tested by a  $\beta$  pulse, in the present context usually of flip angle  $\beta = \pi/2$ , applied in the middle or at the end of the evolution period (Figs. 1B and B'). The variant of

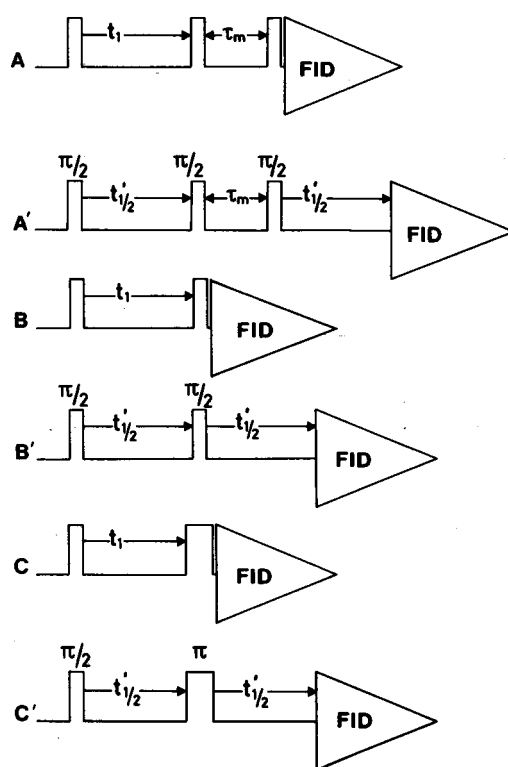


FIG. 1. Experimental schemes of the homonuclear 2D  $^1\text{H}$  NMR experiments which have so far been used for the elucidation of protein conformation. (A, A') 2D NOE spectroscopy (NOESY) without and with delayed accumulation, respectively (3, 10). (B, B') 2D correlated spectroscopy; (B) without delayed accumulation (COSY) (7-9) and (B') with delayed accumulation leading to 2D spin-echo correlated spectroscopy (SECSY) (2, 8). (C, C') 2D  $J$ -resolved spectroscopy without and with delayed accumulation, respectively (1, 6). The evolution time is denoted by  $t_1$  and  $\tau_m$  is the mixing time.

Fig. 1B' with the  $\pi/2$  pulse in the middle of evolution is called 2D spin-echo correlated spectroscopy (SECSY).

(C) 2D *J*-resolved spectroscopy (6, 1) allows the separation of spin-spin multiplets and chemical shifts in two orthogonal frequency dimensions. This may lead to an efficient resolution of overlapping multiplets and allows their detailed analysis. The separation of multiplets and shifts is effected by a  $\pi$  pulse applied during the evolution period (Figs. 1C and C').

For studies of protein structure we have so far primarily used a suitable combination of COSY or (SECSY) and NOESY spectra. 2D *J*-resolved spectroscopy, in addition, may be used for more refined studies of medium-size proteins where the multiplet structure is resolvable. The information contained in the 2D NMR spectra is first used for spectral assignments. In a first step the spin systems of the different amino acid types are identified uniquely or in groups on the basis of the *J*-connectivity patterns in SECSY or COSY spectra recorded in D<sub>2</sub>O (11, 14). Additional support for these identifications may come from determination of the spin-spin coupling fine structure in the 2D *J*-resolved spectra (77). In a second step neighboring residues in the amino acid sequence are identified with NOESY experiments. As shown in Fig. 2 all the crucial <sup>1</sup>H-<sup>1</sup>H connectivities involve the labile backbone amide protons (12-19, 37). It is therefore of critical importance that high-quality NOESY and COSY spectra of proteins can be recorded in H<sub>2</sub>O solution (26, 32). In a third step the data on the identification of amino acid side-chain spin systems and sequential neighborhood relations are combined to obtain individual assignments in the primary structure (13-18, 38).

Once individual resonance assignments have been obtained, all the experiments of Fig. 1 may be useful for obtaining further information on the protein conformation. With regard to determination of three-dimensional polypeptide structures by NMR, NOESY plays a key role by providing a network of short <sup>1</sup>H-<sup>1</sup>H distance

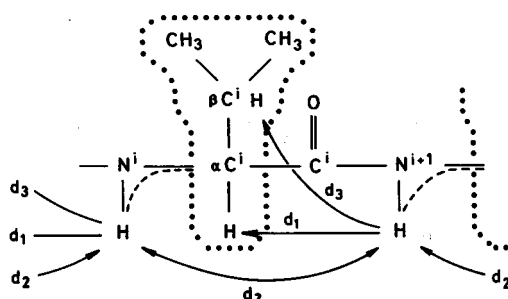


FIG. 2. Peptide segment ---Val---(NH)--- with indication of the *J* and NOE connectivities used to obtain individual resonance assignments for proteins. Dotted lines are drawn around the spin systems of the nonlabile hydrogen atoms in the individual amino acid residues which are identified from the *J* connectivities in SECSY or COSY spectra recorded in D<sub>2</sub>O. The broken lines indicate the *J* connectivities between the backbone amide proton and the  $C^i$  proton of the individual residues, which are determined from COSY or SECSY spectra recorded in H<sub>2</sub>O. The arrows indicate the through-space distances  $d_1$ ,  $d_2$ , and  $d_3$  used to identify sequentially neighboring residues from NOESY spectra recorded in H<sub>2</sub>O (37). Note that  $d_2$  is, in contrast to  $d_1$  and  $d_3$ , symmetrical with respect to the direction of the polypeptide chain.

constraints. These can be used either for interactive model building (39) or as an input for a distance geometry algorithm (40) to develop molecular models which would be compatible with the experimental data. The problem tackled in the distance geometry approach is fundamentally the following (40-42): Given upper limits on the distances between  $N$  atoms by the network of covalent bonds and by the NOESY data, and lower distance limits by the van der Waals radii of the atoms, what are the possible conformations which are compatible with the ensemble of these constraints? Considering that the correlations between peak intensity in the NOESY spectra and proton-proton distances are presently at best semiquantitative (23, 40), it is important that the results of the distance geometry calculations do not depend critically on the accuracy of the distance measurements as long as a sufficiently large number of distance constraints is available (40-42).

For refinement of the structures obtained via the distance geometry approach, these results may be checked against other NMR parameters, such as chemical shifts, spin-spin coupling constants, and amide proton exchange rates (43).  $J$ -coupling constants may be obtained from 2D  $J$  spectra and/or from SECSY and COSY (1, 2, 44, 45). The relative signs of coupling constants become apparent in COSY spectra for flip angles  $\beta < \pi/2$  (7, 9). Again, the data which involve backbone amide protons are of particular interest so that such studies must be based on NMR recordings in  $H_2O$  solution of the proteins.

2D NMR may further provide information on the internal mobility of protein molecules. For example, 2D  $J$  spectroscopy was used to investigate rotational mobility of amino acid side chains about the torsion angle  $\chi^1$ , i.e., about the bond linking  $C^\alpha$  and  $C^\beta$  (Fig. 2) (44), and COSY was employed to measure the exchange rates of individual labile protons in the polypeptide chain with the solvent (21, 22).

Before discussing the relevant practical aspects of the 2D experiments in the following sections, we present in Figs. 3 and 4 representative NOESY and COSY spectra of bull seminal inhibitor IIA (BUSI II A) (18), a protein of molecular weight 6500. The spectra were recorded at 500 MHz on a Bruker WM 500 spectrometer, using the experiments of Fig. 1A for Fig. 3 and of Fig. 1B for Fig. 4. Quadrature detection was employed, with the carrier frequency at the low-field end of the spectrum. To eliminate experimental artifacts, a 16-step phase cycle was used for each value of  $t_1$  (2, 8). The  $H_2O$  resonance was suppressed by selective, continuous irradiation at all times except during data acquisition (26, 32). A total of 512 measurements with  $t_1$  values from 0.3 to 51 msec were recorded with 1024 data points in  $t_2$ . To end up with a 1024 x 1024-point frequency-domain data matrix for COSY and NOESY, which corresponds to the digital resolution given in the figure captions, the time-domain matrix was expanded to 4096 points in  $t_1$ , i.e., 2048 points each for the real and the imaginary part, and 4096 points in  $t_2$  by "zero filling." Prior to Fourier transformation the time-domain data matrix was multiplied in the  $t_1$  direction with a phase-shifted sine bell,  $\sin(\pi(t + t_0)/t_s)$ , and in the  $t_2$  direction with a phase-shifted sine squared bell,  $\sin^2(\pi(t + t_0)/t_s)$ . The length of the window functions,  $t_s$ , was adjusted for the sine bells to reach zero at the last experimental data point in the  $t_1$  or  $t_2$  direction, respectively. The phase shifts,  $t_0/t_s$ , were 1/64 and 1/128 in the  $t_1$  and  $t_2$  directions, respectively. The spectra in Figs. 3 and 4 are shown in the absolute value representation.

The NOESY spectrum in Fig. 3A contains the diagonal peaks on the diagonal

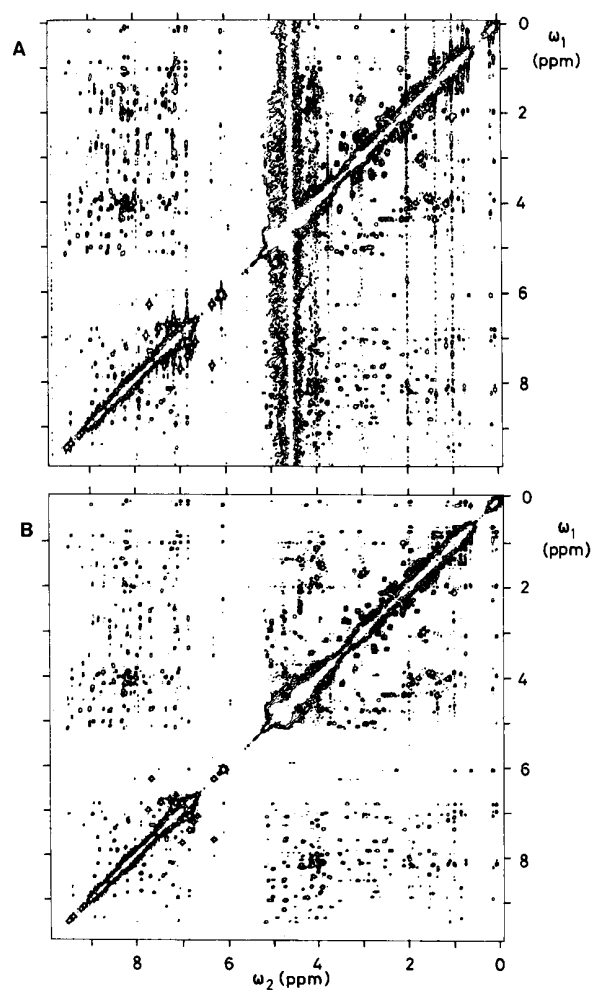


FIG. 3. Contour plot of a 500 MHz  $^1\text{H}$  NOESY spectrum of a 0.016  $M$  solution of bull seminal inhibitor II A (BUSI II A), which is a protein of molecular weight 6500, in  $\text{H}_2\text{O}$ , pH 4.9,  $T = 45^\circ\text{C}$ . The digital resolution is 4.8 Hz/point. The spectrum was recorded in ca. 25 hr. and a mixing time of 200 msec was used. The strong vertical noise band at 4.6 ppm is at the chemical shift of the water resonance, which was suppressed by selective, continuous irradiation at all times except during the acquisition period  $t_2$  (26, 32). (A) unsymmetrized spectrum; (B) spectrum after symmetrization (29).

from the lower left to the upper right corner. These peaks correspond to those in the conventional 1D  $^1\text{H}$  NMR spectrum (3). In addition numerous well resolved cross-peaks occur in all the different spectral regions. These manifest NOEs between protons attached to the same amino acid residue, between sequentially neighboring residues (e.g.,  $d_1$ ,  $d_2$ , and  $d_3$  in Fig. 2) and between residues which are far apart in the amino acid sequence. In NOESY spectra recorded with different mixing times, different relative intensities prevail between the diagonal spectrum and the cross-peaks, and

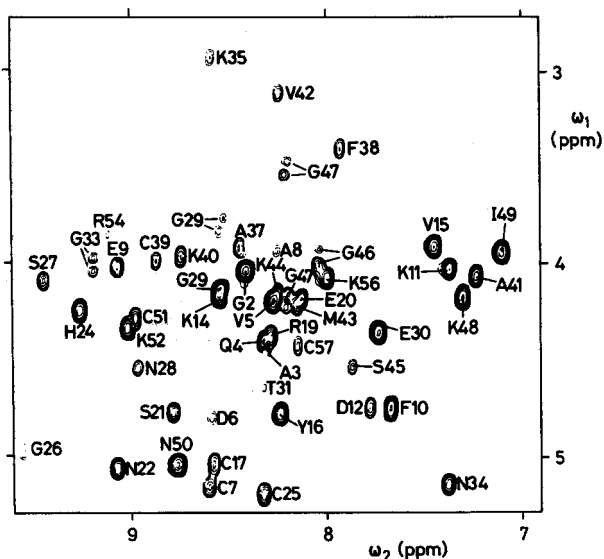


FIG. 4. NMR "fingerprint" of BUSI IIA in the spectral region ( $\omega_1 = 2.8$  to  $5.2$  ppm,  $\omega_2 = 6.9$  to  $9.7$  ppm) of a 500 MHz  $^1\text{H}$  COSY spectrum recorded in a  $0.012$  M solution of the protein in  $\text{H}_2\text{O}$ , pH 4.9, at  $45^\circ\text{C}$ . The digital resolution is 4.8 Hz/point, the spectrum was recorded in ca. 17hr. The water resonance was suppressed by selective, continuous irradiation at all times except during the acquisition period  $t_2$ . The assignments for the individual cross-peaks are indicated by the one-letter symbol for the amino acid residue and the position in the amino acid sequence. Since they were bleached out by the water irradiation (26) the cross-peaks of Thr 18, Tyr 32, His 53, and Gly 55 are missing and the Thr 31 peak is very weak in this spectrum. Furthermore, the cross-peak of Cys 36 is outside of this spectral region at ( $\omega_1 = 2.44$  ppm,  $\omega_2 = 7.92$  ppm) (18).

between different cross-peaks (27). As a rule of thumb for the structural interpretation of the NOESY spectra we assume that the distance between a pair of protons is shorter than ca. 5.0 Å when a NOESY cross-peak can be observed with a mixing time of 100 msec (40). The use of this information is further discussed below.

Figure 3A contains numerous vertical noise bands at the  $\omega_2$  positions of intense diagonal peaks. The most prominent artifacts are at the position of the solvent water resonance. These and additional artifacts can be efficiently suppressed by symmetrization of the spectrum (Fig. 3B) (28, 29). A symmetrized spectrum is usually more practical for the initial spectral analysis and is also more readily amenable for automated peak picking. Potential pitfalls of the technique are discussed in the course of this paper.

A COSY spectrum has the same general appearance as the NOESY spectrum in Fig. 3. It provides with a single instrument setting a complete set of all the scalar spin-spin coupling connections in the macromolecular structure. This includes long-range connectivities with small coupling constants which have in practice not been accessible to 1D  $^1\text{H}$  NMR studies of proteins, e.g., those between the nonlabile imidazole ring protons of histidine (15, 46). The spectral region in Fig. 4 contains the nearly complete "NMR fingerprint" (13) of BUSI II A. The fingerprint of a protein

in the  $C^{\alpha}H-NH$  region of the COSY spectrum contains one peak for each amino acid residue (Fig. 2) except for the prolines, which give no peak, and the glycines, which may give two peaks. When the amino acid sequence is known, inspection of the fingerprint region of the COSY spectrum then shows whether or not the resonances of all the amino acid residues in the protein can be observed and resolved in the  $^1H$  2D NMR spectra (13).

### III. GUIDELINES FOR THE SELECTION OF THE EXPERIMENTAL TECHNIQUE

In setting up a 2D experiment it is at first necessary to select the most appropriate pulse scheme (Fig. 1). This section presents some guidelines.

Each of the three basic experiments shown in Fig. 1 occurs in two variants: Using the same pulse sequence, data acquisition can be started either immediately after the observation pulse ("direct acquisition 2D experiment") or delayed at the time of the expected spin echo ("delayed acquisition 2D experiment") (Fig. 1). In the case of correlated spectroscopy, which is in the following used to further illustrate the two different procedures, this leads to COSY and SECSY, respectively (2, 8). The two types of experiments are to some extent equivalent in the sense that a SECSY spectrum can be computed from a COSY data set while the opposite conversion is only approximately possible since the acquired set for a SECSY-type experiment lacks data in a triangular area of the  $(t_1, t_2)$  domain.

A SECSY-type experiment (with P-type peaks suppressed, see Section IVe) exhibits along  $\omega_1$  only differences of initial and final frequencies and spans a reduced frequency range, provided that all connected peaks are near in the frequency domain. This is always true in 2D  $J$ -resolved spectra of proteins and often true in protein correlation spectra, but happens only rarely in NOESY spectra where cross-peaks appear also between resonance lines which are remote in the frequency domain. SECSY-type experiments are therefore useful particularly for 2D  $J$ -resolved and correlation spectroscopy.

The smaller frequency range to be covered in  $\omega_1$  allows one to save acquisition time and/or permits higher resolution in  $\omega_1$ . The frequency range to be covered in a delayed acquisition experiment should be at least  $\pm(\Delta\omega)_{\max}/2$ , while in the SECSY form of correlated spectroscopy (Fig. 1B')  $(\Delta\omega)_{\max}$  is the maximum frequency difference of/-connected peaks. In 2D  $J$ -resolved spectroscopy (Fig. 1C)  $(\Delta\omega)_{\max}$  is the largest spread of multiplet components in the spectrum (47).

In an echo-type experiment, like SECSY, it is normally impossible to achieve pure absorption and mixed lineshapes are obtained (2, 8). For pure absorption spectra, COSY has to be used with  $\beta = \pi/2$ . However, it should be noted that even with COSY-type experiments a reduced frequency range in  $\omega_1$  of  $\pm(\Delta\omega)_{\max}/2$  is allowed. The resulting foldover can be corrected mathematically with the FOCYSY procedure (foldover-corrected spectroscopy) (8, 48) and leads then to a representation of difference frequencies along  $\omega_1$  which is reminiscent of SECSY-type spectra but can, if required, be recorded in pure absorption. Details on the FOCYSY procedure are presented in Section VI below. From an information-theoretical standpoint FOCYSY appears to be the preferred technique. In practice, a combination of SECSY and COSY spectra of the same protein molecule has proven to be quite efficient for assignment and distinction of incompletely resolved peaks.

## IV. ELIMINATION OF ARTIFACTS AND "UNWANTED" PEAKS

*(a) Elimination of Axial Peaks*

In addition to the cross-peaks of interest and the diagonal peaks (Fig. 3) resonances known as "axial peaks" (7) may appear along the  $\omega_1 = 0$  line in the two-dimensional spectra. These peaks originate from longitudinal magnetization that builds up during the time period immediately before the detection pulse. Such peaks do not contain information of interest and may be eliminated. In a COSY experiment a  $180^\circ$  phase shift of the second rf pulse (mixing pulse) inverts the signs of the axial peaks whereas the signs of the diagonal and cross-peaks are not affected. Addition of the signals from the following two experiments will therefore eliminate axial peaks:

$$\begin{array}{r} x \quad x \quad + \\ x \quad -x \quad +. \end{array} \quad [1]$$

where  $x$  stands for a  $90^\circ_x$ -pulse,  $-x$  for a  $90^\circ_{-x}$  pulse, and  $\pm$  for addition or subtraction of the signals in the computer memory.

In a NOESY experiment, a  $180^\circ$  phase shift of the second pulse inverts the sign of the exchanging  $z$  magnetization. The longitudinal magnetization which builds up during the mixing time and leads to the axial peaks, however, does not change sign. Subtraction of the signals from the following two experiments will thus eliminate axial peaks:

$$\begin{array}{r} x \quad x \quad x \quad + \\ x \quad -x \quad x \quad -. \end{array} \quad [2]$$

*(b) Single and Quadrature Mode Detection*

In 2D NMR spectroscopy of large molecules, performance time and signal to noise ( $S/N$ ) ratio are always limiting factors. It is therefore mandatory to use quadrature phase detection in the  $\omega_2$  direction in order to gain the available factor of 2 in time or  $\sqrt{2}$  in  $S/N$ . In quadrature detection the well-known CYCLOPS sequence (49) should be employed to correct for inaccuracies in the two detector channels and for mismatch of the two audiofrequency filters. Using quadrature phase detection, it is possible to distinguish between positive and negative  $\omega_2$  frequencies (Fig. 5) and to set the carrier frequency in the center of the spectrum for reducing the bandwidth to be covered. This will, however, also cause positive and negative  $\omega_1$  frequencies to occur (Fig. 5) and quadrature detection in  $\omega_1$  will also be necessary. To eliminate image frequencies, two experiments have to be performed for each  $t_1$  value with the rf phases of the mixing pulses shifted by  $\pi/2$  between the two experiments. Because of the large differences between the intensities of diagonal and cross-peaks in COSY and NOESY spectra, the image suppression must be very good to prevent the appearance of a disturbing "antidiagonal" in the resulting 2D spectrum (Fig. 6). Experience shows that this happens frequently in protein spectra. To prevent this, the carrier frequency is often set at one end of the spectrum, but quadrature detection in  $\omega_2$  is nevertheless employed to gain the factor  $\sqrt{2}$  in  $S/N$ . However, image suppression in  $\omega_1$  is then unnecessary.

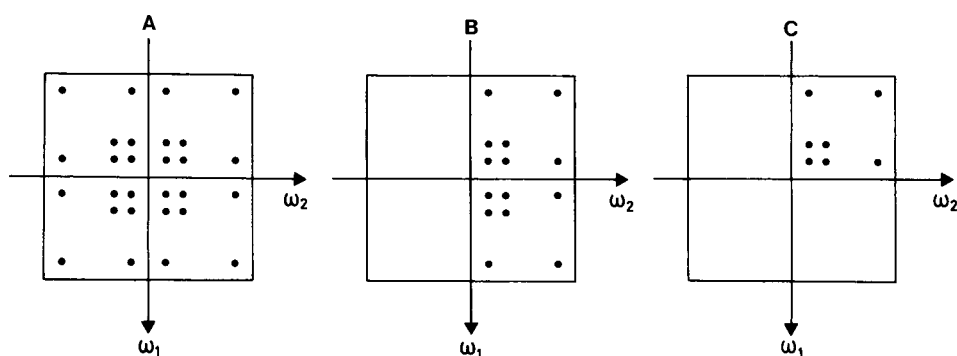


FIG. 5. Scheme illustrating single-channel and quadrature detection in 2D spectroscopy. (A) With single-channel detection the four quadrants in a 2D spectrum cannot be separated. (B) With quadrature detection positive and negative  $\omega_2$  frequencies can be distinguished. (C) By linear combination of two different measurements with different phases of the rf pulses (see text)  $P$  and  $N$  peaks can be distinguished and may be selectively suppressed.

(c) Separation of  $P$ -type and  $N$ -type Peaks

In this section, we discuss in some detail the forementioned problem of quadrature detection in  $\omega_1$ . The application of a mixing pulse of flip angle  $\beta$  between evolution and detection periods (Figs. 1A-C) or in the middle of the evolution period (Figs. 1A'-C') induces transfer of coherence between different transitions as well as between components corresponding to apparently opposite sense of precession during the evolution period  $t_1$ . This leads to pairs of peaks in the 2D spectrum at mirror image frequencies  $\pm\omega_1$ . Peaks which correspond to precession in the same sense in  $t_1$  and

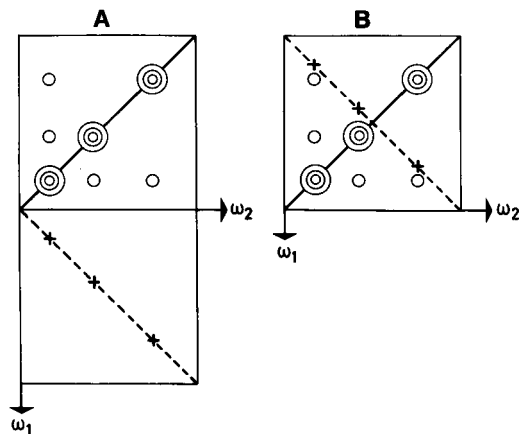


FIG. 6. Suppression of  $P$  peaks. (A) Scheme of a NOESY or COSY spectrum (Figs. 1A and B). The carrier frequency is chosen outside of the spectrum. Quadrature detection along  $\omega_1$  is assumed, with suppression of the  $P$  peaks. Because of incomplete suppression spurious diagonal  $P$  peaks (+) may be retained. (B) When full 2D quadrature detection is applied the spurious peaks are folded into the spectral region of interest and may obscure the spectrum of the  $N$  peaks.

$t_2$  are called *P* peaks (2) or "antiecho peaks," while peaks with precession in opposite sense during  $t_1$  and  $t_2$  are identified as *N* peaks (2) or "echo peaks." The two types of peaks have different character in the presence of magnetic field inhomogeneity; *N*-type peaks tend to be narrower than *P*-type peaks due to refocusing caused by the opposite sense of precession. They have also different flip-angle dependence, *P*-type peaks dominate for small flip angle and disappear for  $\beta = \pi$  while *N*-type peaks have vanishing amplitude for  $\beta = 0$  and become maximum for  $\beta = \pi$ . For  $\beta = \pi/2$ , the two kinds have equal amplitude.

Complete COSY and SECSY spectra for an AMX spin system are shown in schematic form in Figs. 7 and 8. It is obvious that only the *N*-type peaks in a SECSY spectrum exhibit the advantage of a restricted  $\omega_1$  frequency range. There is thus a strong motivation to devise experimental schemes by which the *P*-type peaks can be suppressed. Another reason for separation is the severe overlap of the two classes of peaks whenever the rf carrier is set in the center of the spectrum.

Suppression of one of the two classes of peaks is possible by a set of experiments with a suitable phase cycle. For a COSY experiment the following two experiments have to be combined

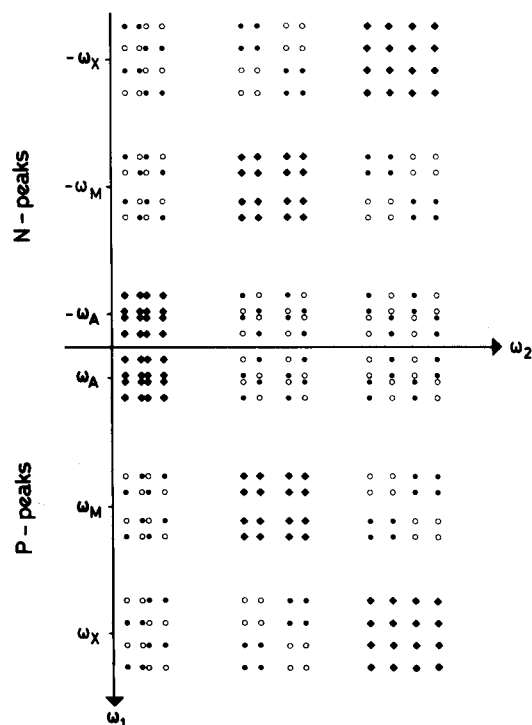


FIG. 7. Schematic COSY spectrum of an AMX spin system; weak coupling is assumed. The coupling constants are  $J_{AM} = 5$  Hz,  $J_{AX} = 7$  Hz, and  $J_{MX} = -14$  Hz. Positive absorptive ( $\bullet$ ), negative absorptive ( $\circ$ ), and dispersive ( $*$ ) resonance lines are distinguished. All absolute-value intensities are equal. Note that this AMX system, which is important in protein  $^1\text{H}$  NMR spectra (44), contains different groups of cross-peaks with identical signs.

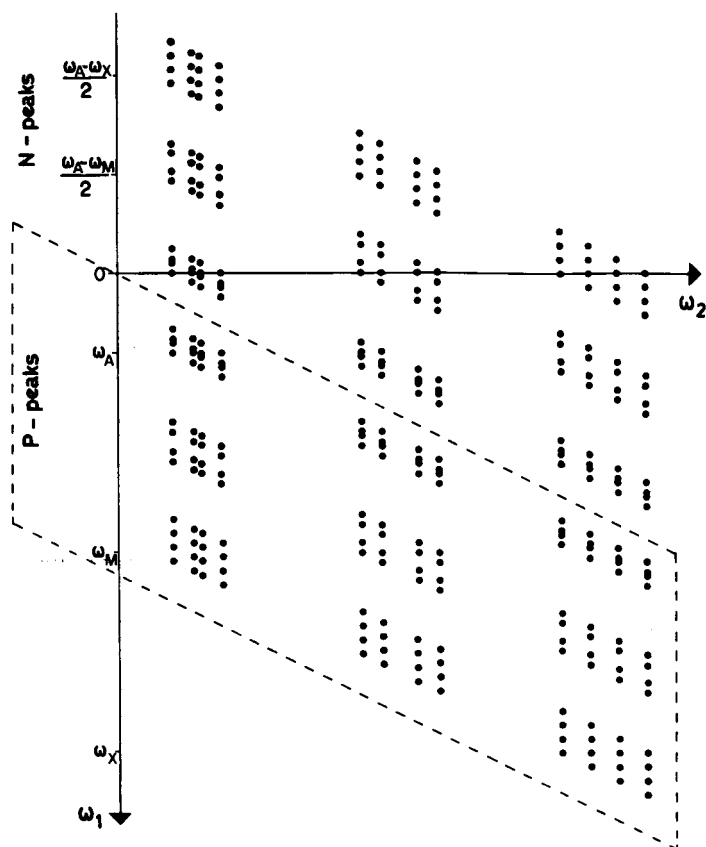


FIG. 8. Schematic SECSY spectrum of an AMX spin system. The coupling constants are  $J_{AM} = 5$  Hz,  $J_{AX} = 7$  Hz, and  $J_{MX} = -14$  Hz and weak coupling is assumed. All peaks in a SECSY spectrum consist of a superposition of an absorptive and a dispersive contribution. Cross-peak multiplets are in antiphase such that severe overlap leads to cancellations. SECSY spectra are normally plotted in absolute-value mode.

		$N$	$P$	
$x$	$x$	+	+	[3]
$x$	$y$	-	+	

Here  $x$  and  $y$  indicate the phases of the applied rf pulses while  $\pm$  refers to addition or subtraction of the signals to obtain either  $N$ - or  $P$ -type peaks. Combined with the suppression cycle for axial peaks of Eq. [1], the following phase cycle is obtained:

		$N$	$P$	
$x$	$x$	+	+	[4]
$x$	$y$	-	+	
$x$	$-x$	+	+	
$x$	$-y$	-	+	

which is also called EXORCYCLE (50). An experimental example of an AMX system is shown in Fig. 9. Figure 9A gives the complete SECSY spectrum without separation of *N*- and *P*-type peaks while in Fig. 9B the *P*-type peaks have been suppressed by the cycle of Eq. [4].

For NOESY experiments cycle [4] can be used as well. The two mixing pulses use the same phase as the second pulse in cycle [4]. For quadrature detection in both directions the phase cycles must be combined with CYCLOPS (49) to compensate for phase and amplitude errors. In the notation used here CYCLOPS is written as

$$\begin{array}{l} x \quad +A \quad +B \\ y \quad -B \quad +A \\ -x \quad -A \quad -B \\ -y \quad +B \quad -A. \end{array} \quad [5]$$

The signals *A* and *B* of the two detectors are added (+) or subtracted (-) into two memory regions in the computer. The two memory regions are indicated by the second and third column in [5]. The combination of phase cycles [4] and [5] leads to a cycle with 16 phases for both COSY and for NOESY (Tables 1 and 2). The application of the full scheme is necessary when the carrier frequency is set in the middle of the spectrum, otherwise partial schemes may profitably be employed (see footnotes to Tables 1 and 2).

#### (d) Setting the Carrier Frequency

In a polypeptide or protein 2D spectrum many of the cross-peaks have only a few percent of the intensity of the diagonal peaks. Mirror image diagonal peaks in quadrature detection (Fig. 6) can therefore be quite disturbing even when the quadrature balance is well adjusted. For this reason it is often advisable in COSY and NOESY experiments to set the carrier frequency to one end of the spectrum even when quadrature detection is available. An additional advantage is that incompletely suppressed axial peaks do then not appear in the central region of the 2D spectrum.

In SECSY experiments, where the *P* peaks must always be suppressed, frequency

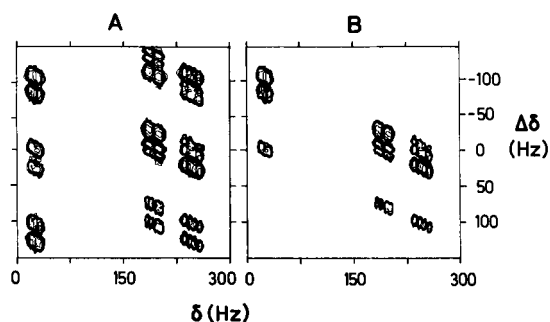


FIG. 9. SECSY spectrum of a 0.04 *M* tyrosine solution in D<sub>2</sub>O, pD = 11.5, *T* = 30°C. The spectral region is shown which contains the resonances of the C<sup>α</sup>H-C<sup>β</sup>H<sub>2</sub> AMX spin system. (A) *N*- and *P*-type peaks are present. Some of the *P* peaks are folded in the  $\omega_1$  direction. (B) Only the *N*-type peaks are present, the *P* peaks have been suppressed.

TABLE 1

PHASE CYCLE FOR HOMONUCLEAR 2D  
CORRELATED SPECTROSCOPY (COSY/SECSY)  
ALLOWING FULL QUADRATURE DETECTION  
(AXIAL AND P PEAKS ARE SUPPRESSED)<sup>a</sup>

Phases		Computer memory	
1st Pulse	2nd Pulse	Region I	Region II
<i>x</i>	<i>x</i>	+ <i>A</i>	+ <i>B</i>
<i>x</i>	- <i>x</i>	+ <i>A</i>	+ <i>B</i>
<i>y</i>	<i>y</i>	- <i>B</i>	+ <i>A</i>
<i>y</i>	- <i>y</i>	- <i>B</i>	+ <i>A</i>
- <i>x</i>	- <i>x</i>	- <i>A</i>	- <i>B</i>
- <i>x</i>	<i>x</i>	- <i>A</i>	- <i>B</i>
- <i>y</i>	- <i>y</i>	+ <i>B</i>	+ <i>A</i>
- <i>y</i>	<i>y</i>	+ <i>B</i>	+ <i>A</i>
<i>x</i>	<i>y</i>	- <i>A</i>	- <i>B</i>
<i>x</i>	- <i>y</i>	- <i>A</i>	- <i>B</i>
<i>y</i>	- <i>x</i>	+ <i>B</i>	- <i>A</i>
<i>y</i>	<i>x</i>	+ <i>B</i>	- <i>A</i>
- <i>x</i>	- <i>y</i>	+ <i>A</i>	+ <i>B</i>
- <i>x</i>	<i>y</i>	+ <i>A</i>	+ <i>B</i>
- <i>y</i>	<i>x</i>	- <i>B</i>	+ <i>A</i>
- <i>y</i>	- <i>x</i>	- <i>B</i>	+ <i>A</i>

<sup>a</sup> The schemes [1], [3] and [5] are the basis for this phase cycle. Application of the full sequence of 16 phases is needed for recording of absolute-value spectra when the carrier is in the center of the spectrum. When the carrier frequency is set to one end of the spectrum only the first block of 8 phases is profitably employed. The data can then be transformed in either the absolute-value mode or the phase sensitive mode. Use of the full scheme of 16 phases results in mixing of absorptive and dispersive lineshapes and phase-sensitive spectra can only be obtained when the recordings with the first and second cycle of 8 phases are stored in separate memory locations. This allows one to obtain phase-sensitive spectra from recordings with a centrally located carrier frequency (76-78).

folding of spurious *P*-type peaks cannot be avoided and there is no particular reason not to set the carrier frequency in the center of the spectrum. In 2D *J*-resolved spectroscopy, it is convenient to set the carrier frequency in the center of the spectrum. *P*-type peaks do not occur in this case provided that the 180° pulse is perfect.

(e) *Suppression of J Cross-Peaks and Transverse Magnetization in NOESY*

For the proper functioning of a NOESY experiment exclusively frequency-labeled longitudinal magnetization should exist during the mixing period. Additional com-

TABLE 2  
 PHASE CYCLE FOR 2D NOE SPECTROSCOPY (NOESY)  
 ALLOWING FULL QUADRATURE DETECTION  
 (AXIAL AND *P* PEAKS ARE SUPPRESSED) AND  
 REMOVING TRANSVERSE MAGNETIZATION<sup>a</sup>

Phases		Computer memory	
1st Pulse	2nd Pulse	Region I	Region II
<i>x</i>	<i>x</i>	+ <i>A</i>	+ <i>B</i>
<i>x</i>	- <i>x</i>	- <i>A</i>	- <i>B</i>
<i>x</i>	<i>x</i>	- <i>B</i>	+ <i>A</i>
<i>x</i>	- <i>x</i>	+ <i>B</i>	- <i>A</i>
<i>x</i>	<i>x</i>	- <i>A</i>	- <i>B</i>
<i>x</i>	- <i>x</i>	+ <i>A</i>	+ <i>B</i>
<i>x</i>	<i>x</i>	+ <i>B</i>	- <i>A</i>
<i>x</i>	- <i>x</i>	- <i>B</i>	+ <i>A</i>
<i>x</i>	<i>y</i>	- <i>A</i>	- <i>B</i>
<i>x</i>	- <i>y</i>	+ <i>A</i>	+ <i>B</i>
<i>x</i>	<i>y</i>	+ <i>B</i>	- <i>A</i>
<i>x</i>	- <i>y</i>	- <i>B</i>	+ <i>A</i>
<i>x</i>	<i>y</i>	+ <i>A</i>	+ <i>B</i>
<i>x</i>	- <i>y</i>	- <i>A</i>	- <i>B</i>
<i>x</i>	<i>y</i>	- <i>B</i>	+ <i>A</i>
<i>x</i>	- <i>y</i>	+ <i>B</i>	- <i>A</i>

<sup>a</sup>The phase cycles discussed in Section IVc are the basis of this table. See footnote to Table 1.

ponents, like transverse magnetization and multiple-quantum coherence, will lead to artifacts in the NOESY spectrum in the form of incorrect intensities and phases, and in the appearance of *J* cross-peaks (10, 51). The elimination of all unwanted components, except for zero-quantum coherence, is quite easy and can be achieved either by the application of a field gradient pulse during the mixing period (10) or much better by a suitable phase cycle (57). Phase cycle [2], for example, eliminates all odd order multiple-quantum transitions. The phase cycle of Table 2 suppresses in addition effects from double-quantum coherence. Zero-quantum coherence can, however, not be removed by phase cycling. Unfortunately, it contributes significantly to the *J* cross-peaks in polypeptide spectra (31).

The elimination of zero-quantum coherence can utilize its rapid oscillation during the mixing time (30, 52). A random modulation (52) of the mixing time,  $\tau_m$  (Fig. 1A), within a selected interval  $\tau_m^{\text{var}}$  averages zero-quantum coherence nearly to zero provided that  $\tau_m^{\text{var}}$  extends over several oscillation periods (determined by chemical shift differences). NOE cross-peaks are only insignificantly affected by such a variation of  $\tau_m$ . The insertion of a 180° pulse with variable position in the mixing period has a similar effect as the variation of the mixing time (31). The random variation of the mixing time (or the 180° pulse position) must cover time intervals longer than one period of the lowest zero-quantum transition frequency

$$\tau_m^{\text{var}} > 1/\omega_{\text{min}}^{\text{ZQT}}. \quad [6]$$

$1/\omega_{\text{min}}^{\text{ZQT}}$  is equal to the smallest chemical shift difference  $\Delta\omega$  between coupled nuclei. In practice this means that  $\tau_m^{\text{var}}$  must be of the order of 2-10 msec to cover the low-frequency range from 100-500 Hz.

Instead of a random variation of the mixing time  $\tau_m$  or of the position of the  $180^\circ$  pulse, a systematic incrementation of the mixing time correlated with the increase of  $t_1$  can also be employed (30, 31)

$$\tau_m = \tau_m^0 + (k/N) \tau_m^{\text{var}}; \quad k = 0, 1, \dots, N. \quad [7]$$

This leads to a shift displacement of the  $J$  cross-peaks in the  $\omega_1$  direction, leaving exclusively the NOE cross-peaks in place. By a symmetrization of the 2D spectrum (28, 29) it is then possible to eliminate the  $J$  cross-peaks efficiently.

*(f) Suppression of the Solvent Line in H<sub>2</sub>O Solutions of Proteins*

In <sup>1</sup>H NMR experiments with H<sub>2</sub>O solutions of proteins, which are of crucial importance in structural studies (see Section II), one faces severe problems with regard to detecting weak resonance signals in the presence of a strong solvent line. Since for proteins the experimental conditions can usually be selected such that magnetization transfer with the solvent by exchange of the amide protons is inefficient (43, 53), this problem can be circumvented by selective saturation of the solvent resonance (26). Among different water suppression schemes that have been used (12-19, 26, 32), the experiment shown in Fig. 10 appears to be the best choice. A continuous, selective rf field is applied to the H<sub>2</sub>O line at all times except during the periods  $t_1$  and  $t_2$ , which have to be chosen sufficiently short so that no significant recovery of the water magnetization occurs. The effect of the solvent suppression is illustrated in Fig. 11. Without suppression of the water line, the signal to noise ratio is such that (with the possible exception of two or three particularly strong peaks) the positions of the cross-peaks cannot be determined (compare Fig. 11A with Figs. 11B and C).

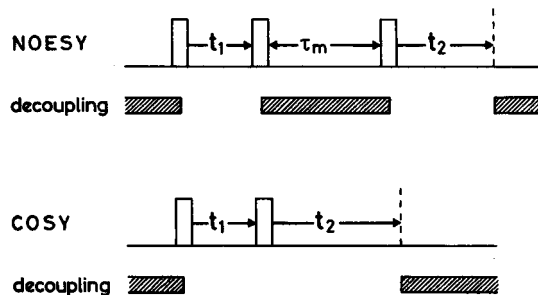


FIG. 10. Experimental scheme for the H<sub>2</sub>O suppression in COSY and NOESY experiments. The H<sub>2</sub>O resonance is continuously irradiated at all times except during  $t_1$  and  $t_2$ . Compared to the procedure used for the experiments of Figs. 3 and 4, where the decoupler was on also during  $t_1$ , this scheme has the advantage that no Bloch-Siegert shifts will distort the spectrum even at high amplitudes of the decoupler field.

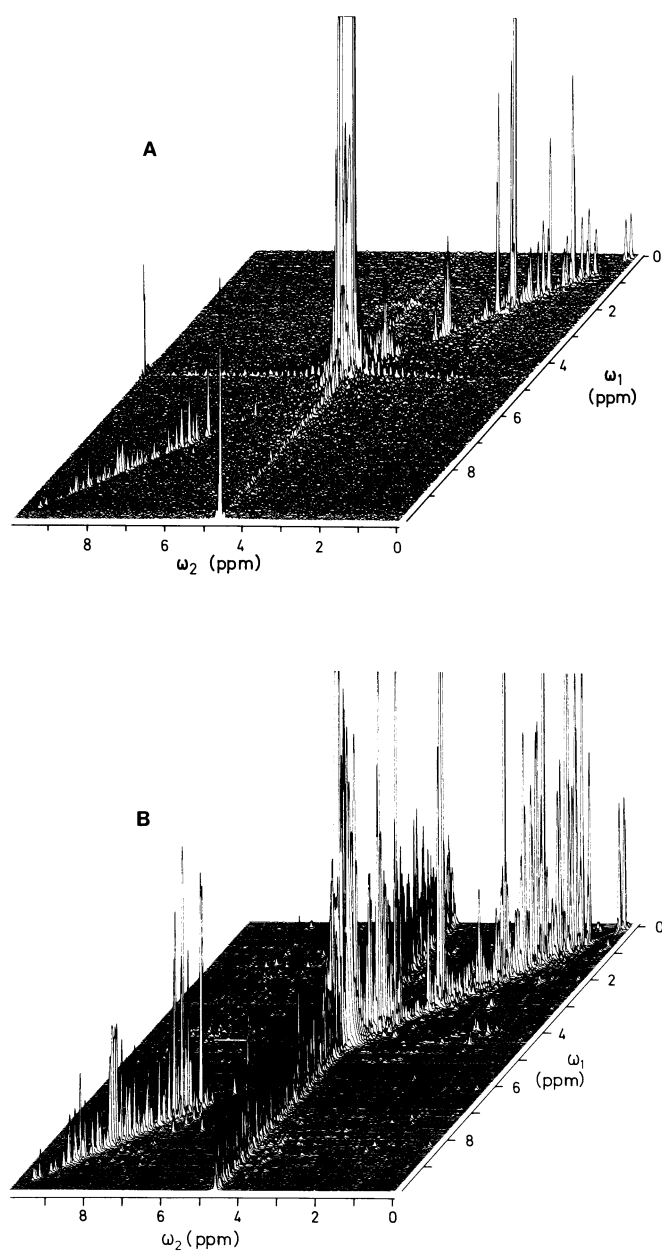


FIG. 11. Stacked plot presentation of three 500 MHz  $^1\text{H}$  NOESY spectra of the BUSI II A solution used in Fig. 3. (A) Spectrum recorded without water suppression. (B) Spectrum recorded with water suppression (same data as in Fig. 3A). (C) Spectrum B after symmetrization (same data as in Fig. 3B). For all three spectra identical experimental parameters were used with the exception of the solvent suppression and symmetrization mentioned above.

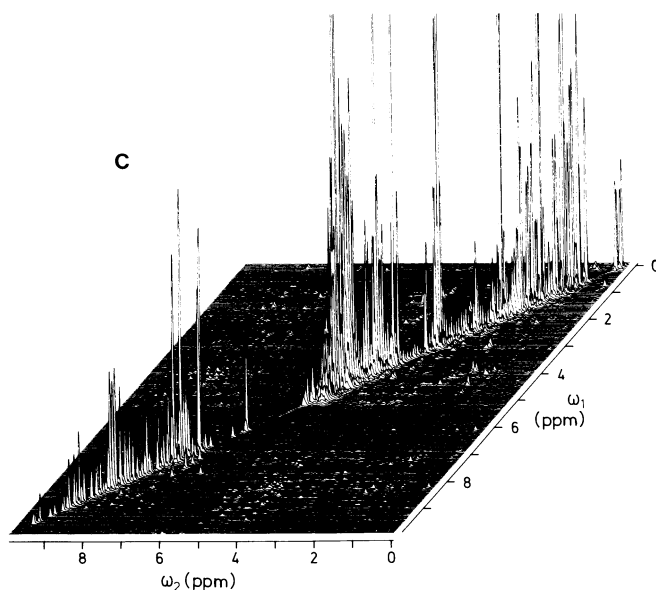


FIG. 11—Continued.

Solvent suppression normally leaves some residual perturbations in the spectrum. Thus a strong ridge parallel to the  $\omega_1$  axis at the water resonance originates from incomplete saturation of the solvent line, which may differ slightly from experiment to experiment (Fig. 3A and 11B). Furthermore, protein resonances near the water line may also be saturated, and as a consequence cross-peaks with these lines may disappear from the spectrum (26). These difficulties can be minimized by optimization of the field homogeneity, since the better the field homogeneity the less rf power is needed for effective solvent suppression. As a result a weaker ridge is obtained and a minimal number of cross-peaks is bleached out. With regard to the latter effect it is also possible to exploit the large temperature coefficient of the chemical shift of water (43). By a suitable choice of the temperature the water line can often be placed in an otherwise empty region of the spectrum, or a complete set of cross-peaks can be obtained by two complementary measurements at different temperatures (26).

Besides the experiment of Fig. 10, a suppression scheme which we recently used (e.g., Figs. 3, 4, and 11B and C) consists of continuous irradiation at all times except during  $t_2$  (32). Fundamentally this provides for a more complete solvent suppression, but there is the disadvantage that unless a weak rf field can be applied, the 2D NMR spectra may be distorted by Bloch-Siegert shifts (32). A numerical correction of the Bloch-Siegert shifts in COSY and NOESY spectra has recently been described (33).

The well-known Redfield solvent suppression technique (54), offers an alternative but more delicate procedure. It has the significant advantage that cross-peaks to resonances coinciding with the solvent line are not suppressed and even more important that protons which are chemically exchanging with the solvent can also be observed. This is crucial when rapid exchange of labile protons is studied by a 2D chemical exchange experiment (55). In work with biopolymers, this type of suppression scheme

may be needed for experiments with proteins at high temperature and high pH, and quite generally for studies of nucleic acids (43, 54).

#### V. SELECTION OF PERFORMANCE PARAMETERS

A 2D experiment differs from a 1D experiment in that experiments for a large number  $X_1$  of equidistant  $t_1$  values, with an increment  $\Delta t_1$  have to be performed. The increment  $\Delta t_1$  is determined by the maximum frequency range  $\omega_{1\max}$  to be covered through the sampling theorem,

$$\Delta t_1 < 1/(2\omega_{1\max}). \quad [8]$$

In direct acquisition 2D experiments (Figs. 1A-C), the spectral ranges in  $\omega_1$  and  $\omega_2$  are the same. In a SECSY experiment  $\omega_{1\max}$  is equal to half the largest frequency difference between coupled nuclei. In protein spectra, alanine and threonine usually set the upper limit, with roughly 4 ppm chemical shift difference between coupled protons. In delayed acquisition 2D  $J$ -resolved spectra, a value  $\omega_{1\max}$  of  $\pm 20$  to  $\pm 30$  Hz is normally sufficient if strong coupling effects are neglected (47). For FOCYSY the same considerations apply as for the corresponding delayed acquisition experiments.

The number  $X_1$  of  $t_1$  values determines the resolution in  $\omega_1$ , and obviously at the same time the total performance time.  $X_1$  also influences the  $S/N$  ratio when the sampling process is extended too far into the  $t_1$  decay of the signal. In any case, apodization in  $t_1$  is equally important as in  $t_2$ . Table 3 shows some parameters which are routinely applied on a 500 MHz spectrometer for measuring protein 2D  $^1\text{H}$  NMR spectra. For 10 mM protein solutions in 5 mm sample tubes, spectra with acceptable  $S/N$  ratio are obtained in about 10 to 24 hr. The maximum value of  $X_2$  is usually determined by the disk storage capacity. The relaxation delay can be correspondingly shorter when more  $t_2$  data points are acquired.

Before starting a 2D experiment a precise calibration of the 90 and 180° pulse

TABLE 3  
SAMPLES OF PARAMETERS USED FOR RECORDINGS OF RELATIVELY "LOW RESOLUTION"  
2D  $^1\text{H}$  NMR EXPERIMENTS AT 500 MHz<sup>a</sup>

2D Experiment	$\pm\omega_{1\max}/2\pi$ (Hz)	$\pm\omega_{2\max}/2\pi$ (Hz)	$X_1^b$	$X_2^b$	Hz/pt <sup>b</sup>	
					$\omega_1/2\pi$	$\omega_2/2\pi$
2D $J$ (Fig. 1C')	20	4000	64	4096	0.6	2
SECSY (Fig. 1B')	1000	4000	512	3072	4	2.6
COSY <sup>c</sup> (Fig. 1B)	5000	10000	512	2048	20	10
NOESY <sup>c</sup> (Fig. 1A)	5000	10000	512	2048	20	10

<sup>a</sup> The values given are useful for small diamagnetic proteins with molecular weight up to ca. 15,000 (for bigger proteins the choice of parameters will in general have to be reconsidered). With these parameters and a relaxation delay of 1.5 sec a spectrum with good  $S/N$  ratio of a 10 mM protein solution can be recorded in ca. 10 to 24 hr.

<sup>b</sup>  $X_1$ , number of  $t_1$  values;  $X_2$ , number of sampling points in each FID; Hz/pt, resolution in  $\omega_1$  and  $\omega_2$  without zero filling.

<sup>c</sup> For COSY and NOESY it is assumed that the carrier frequency is set to one end of the spectrum.

angles is needed. Whenever possible the calibration should be made with the sample to be measured, because the pulse angle may depend on experimental parameters such as the solvent, the salt concentration, and the sample temperature.

Special care has to be taken to properly adjust the receiver gain in 2D experiments to avoid overflow because the first experiment with  $t_1 = 0$  does not necessarily produce the largest signal. Consider, for example, a COSY experiment with two  $90^\circ$  pulses. For  $t_1 = 0$  the two  $90^\circ$  pulses act like a  $180^\circ$  rotation which generates no signal at all. For a setup experiment, it is advisable to apply a single  $90^\circ$  pulse to the sample to be studied and use the resulting signal amplitude as a measure for the expected signal maximum.

Normally, many scans have to be averaged for each  $t_1$  value. Here the question arises whether it is advantageous to cycle first through all  $t_1$  values before the next repetition or whether all experiments for one  $t_1$  value should be performed in sequence. To our experience there is no advantage to cycle several times through all  $t_1$  values. Such a procedure would have the disadvantage that in case of a system failure (e.g., lost lock) toward the end of the experiment the entire experiment may be destroyed, whereas in a consecutive experiment only the samples for longer  $t_1$  would be lost, resulting merely in a slightly reduced resolution.

A special comment concerns the choice of the mixing time,  $\tau_m$ , in NOESY experiments (Fig. 1A and A'). The  $\tau_m$ -dependence of NOESY was investigated for the basic pancreatic trypsin inhibitor (BPTI) (27) and for micelle-bound glucagon (23). For BPTI a plot of the peak intensities vs  $\tau_m$  (Fig. 5 of Ref. (27)), which is representative for the  $\tau_m$  dependence of NOESY spectra of small proteins, showed a monotonous decrease of the diagonal peak intensity. Two different types of behavior were observed for different cross-peaks. Some cross-peaks showed rapid growth at short  $\tau_m$  values, reached a maximum intensity after 150 to 200 msec and subsequently decayed at still longer mixing times. For other cross-peaks the intensity started to increase after a lag period of up to ca. 100 msec, indicating that the magnetization transfer was dominated by "spin diffusion" (27). For conformational studies of proteins it is therefore advisable to collect several NOESY spectra with different mixing times, so that spin-diffusion processes can be identified and separated from "direct" NOEs, which provide more reliable distance information. In practice, mixing times between 30 and 200 msec have been used (12-19, 23, 27). On principal grounds measurements with very short mixing times are of prime interest for measurements of  $^1\text{H}$ - $^1\text{H}$  distances. However, the interpretation of such spectra is often limited by the appearance of intense bands of " $t_1$  noise" (Fig. 3A) and depends crucially on efficient  $J$ -peak suppression (see Section IVe). We found it helpful to record a spectrum with a long mixing time of ca. 200 msec, where the location of the cross-peaks can be accurately determined, and to use this spectrum as a guide for the interpretation of the data obtained with short mixing times (23).

## VI. DATA PROCESSING

### (a) Data Manipulation before 2D Fourier Transformation

In two-dimensional spectroscopy filtering procedures have to be applied in both frequency domains. Normally the Fourier transformation is executed in two steps,

first with respect to  $t_2$  and then with respect to  $t_1$ . Filtering in  $\omega_2$  can be performed by multiplication of the original  $s(t_1, t_2)$  data with a suitable weighting function  $h_2(t_2)$ , while filtering in  $\omega_1$  is applied most conveniently prior to the second Fourier transformation by multiplication of the  $S(t_1, \omega_2)$  data with a weighting function  $h_1(t_1)$ .

(i) *Baseline correction.* Baseline correction by subtracting a constant or a linearly increasing function from the original data is a standard operation in 1D spectroscopy. In 2D spectroscopy, it must be used with care. In particular, the same correction should be applied to all FIDs in  $s(t_1, t_2)$  or  $S(t_1, \omega_2)$ . If individual baseline corrections are used, differing from FID to FID, artifacts may arise. In addition, signals at  $\omega_1 = 0$  or  $\omega_2 = 0$  may be lost or suppressed by application of a baseline correction. As an illustration Fig. 12 shows the suppression of an axial peak by the use of a baseline correction in the  $t_1$  domain.

(ii) *Resolution enhancement.* One-dimensional and two-dimensional protein  $^1\text{H}$  NMR spectra invariably win when moderate digital resolution enhancement is applied. Resolution enhancement is indispensable when absolute-value spectra are displayed to reduce the broad signal tails originating from the dispersive parts. As in 1D spectroscopy digital filtering is performed by multiplication of the time-domain data by a suitable filtering function (56, 57). The multiplication in the two time domains is usually performed independently, possibly with different filtering functions. All suitable resolution enhancement functions  $h(t)$  start for  $t = 0$  at a low value, increase to a maximum and fall off towards the end, preferentially to zero. The initial low values suppress broad signal components, the intermediate maximum is responsible for the enhancement of narrow lines, and the ultimate fall-off avoids truncation errors by apodization and maintains an acceptable  $S/N$  ratio by attenuating the noisier parts of the FID. Various suitable weighting functions can be found in the literature (43, 56-58).

A good compromise between resolution enhancement and sensitivity can be achieved by applying a Lorentz-Gauss transformation (56) which is theoretically justified for

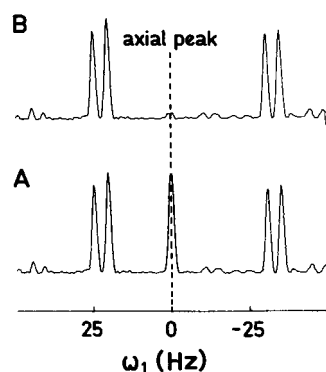


FIG. 12. Suppression of axial peaks at  $\omega_1 = 0$  by application of a baseline correction. The same cross section through a  $^1\text{H}$  COSY spectrum of 2,3,4-trichlorophenol is shown in the two traces. (A) No baseline correction was used and there appears an intense axial peak. (B) After the baseline correction the axial peak is almost completely suppressed. The carrier frequency has been set within the recorded spectral range.

Lorentzian lines, i.e., for exponential FIDs. Another concept is based on the idea of a "pseudo-echo" (59). It allows the exact suppression of dispersive parts and leads to similar weighting functions. A further, empirical approach utilizes sine-bell functions (58). The sine bell or in an improved version a shifted sine bell (60) is very easily generated and applied. It requires specification of a single parameter only, the time shift. Another function with the same virtue is the squared sine-bell function which approaches the Lorentz-Gauss transformation. In 2D  $^1\text{H}$  NMR of proteins, the use of shifted sine-bell and shifted squared sine-bell functions was found convenient and efficient (e.g., Figs. 3, 4, and 11 and Refs. (13-19)) and no need for a more profoundly justified weighting function became apparent.

The influence of different digital filtering functions on a protein 2D  $^1\text{H}$  NMR spectrum is illustrated in Fig. 13. The three spectra were obtained from the same data set by applying different filtering functions. The result of a cosine apodization, which eliminates truncation errors but does not provide resolution enhancement, is shown in Fig. 13A. This spectrum is hardly suitable for analysis. The best result was obtained with the squared sine-bell filter (Fig. 13B), which adopts zero value for  $t = 0$  (Fig. 13B), whereas the Lorentz-Gauss transform for the chosen parameter set is less efficient in suppressing broad lines (Fig. 13C). Comparison of Figs. 13B and C affords an illustration of how critical the selection of the filter functions can be, in particular when absolute value presentations are used.

(iii) *Zero filling.* In two-dimensional protein spectroscopy, the available performance time invariably sets an upper limit to the number of  $t_1$  values which can be measured. To improve the visual appearance of the resulting spectra, zero filling (61), particularly in the  $t_1$  domain, is required in almost all cases. Experience with protein  $^1\text{H}$  NMR spectra showed that  $N$  data points can be supplemented by up to  $3N$  zero values with a noticeable improvement of resolution, further zero filling is ineffective. In Fig. 14 spectra with different zero filling prior to the Fourier transformation illustrate this point.

#### (b) Data Manipulation after 2D Fourier Transformation

(i) *Triangular multiplication and symmetrization.* Ideal COSY and NOESY spectra are symmetrical with respect to the main diagonal  $\omega_1 = \omega_2$ . In practice, however, noise and instrumental artifacts destroy the symmetry (Figs. 3A and 11B). By a suitable combination of the upper left and the lower right triangle, it is possible to improve the significance of a 2D spectrum (Figs. 3 and 11). One possibility is calculating the geometric mean (28) of upper and lower triangles ("triangular multiplication"). In another procedure of "triangular symmetrization," the lower one of each pair of symmetrically located values is retained (29). A slight improvement of the  $S/N$  ratio can at the same time also be achieved with these procedures (28, 29). Furthermore, triangular symmetrization is important for  $J$  cross-peak elimination from NOESY spectra after application of the  $\tau_m$  incrementation method (30) (see Section IVe).

We should note that symmetrization may lead to erroneous peaks when the original spectrum contains strong ridges extending parallel to one of the two axes. The crossing of two ridges in the symmetrization process will feign the presence of two symmetrically located peaks. Such artifactual peaks can, for example, be found in Figs. 3B and 11C

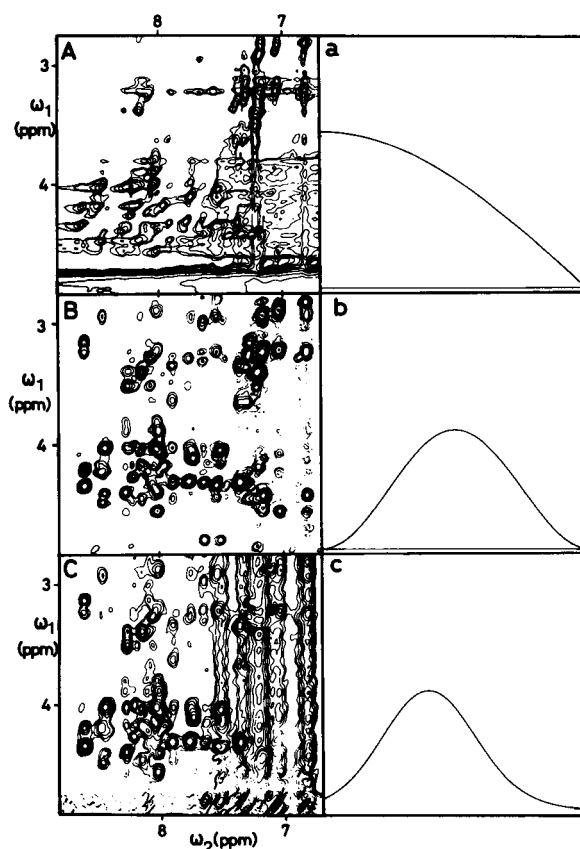


FIG. 13. Improvement of 2D  $^1\text{H}$  NMR spectra of proteins by multiplication of the time-domain data with different resolution enhancement functions. (A) to (C) show the region ( $\omega_1 = 2.8 - 4.9$  ppm,  $\omega_2 = 6.7 - 8.8$  ppm) from a 500 MHz  $^1\text{H}$  NOESY spectrum recorded with a mixing time of 200 msec at 37°C in a  $\text{H}_2\text{O}$  solution which contained the polypeptide hormone glucagon bound to micelles of perdeuterated dodecyl phosphocholine (0.015 M glucagon, 0.7 M [ $^2\text{H}_{38}$ ]dodecylphosphocholine, 0.05 M phosphate buffer, pH 6.0). The  $\text{H}_2\text{O}$  resonance was suppressed by continuous irradiation at all times except during  $t_2$ . The glucagon-containing micelles have a molecular weight of ca. 17,000 (14) and correspondingly the  $^1\text{H}$  NMR lines are quite broad. (A) The time-domain data matrix was multiplied with the cosine function a. (B) Multiplication with the sine squared function b. (C) Multiplication with the Gaussian function c.

for which the crossings of the strong water ridge with the weaker  $t_1$ -noise bands of the methyl groups are responsible. In such cases it is advisable to compare symmetrized and original spectra. It is obvious that symmetrization has also its limitation when the  $S/N$  ratio is below a certain limit. It is not possible to retrieve signals which are smaller than the noise level, and accidental coincidences of strong noise peaks can never be excluded.

(ii) *Foldover-corrected spectroscopy (FOCSY)*. It has been mentioned in Section III that foldover correction of a conventional COSY spectrum can be used as an alternative to SECSY. It permits the same optimized usage of performance time, data storage, and resolution in the  $\omega_1$  domain. Foldover in  $\omega_1$  caused by a low sampling

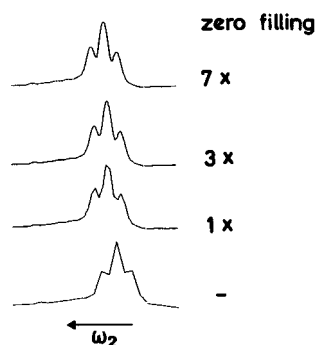


FIG. 14. Influence of "zero filling" in the time domain on the appearance of the frequency-domain spectrum. The numbers on the right indicate the extent of the zero filling relative to the number of experimental data points. There is no use to supplement  $N$  data points by more than  $3N$  zeros.

rate in  $t_1$ , violating the sampling theorem, can be corrected whenever all cross-peaks are located within a range of  $\pm\omega_N$  from the main diagonal (8). The rearrangement of the originally folded spectrum  $S(\omega_1, \omega_2)$  into a foldover-corrected spectrum  $S'(\omega_1', \omega_2')$  can be formulated as (8)

$$S'(\omega_1', \omega_2') = S(\omega_1, \omega_2) \quad [10]$$

with

$$\omega_1' = (\omega_1 - \omega_2 + \omega_N) \bmod (\omega_N) - \omega_N$$

$$\omega_2' = \omega_2$$

where  $\omega_N$  stands for the Nyquist frequency. Figure 15 presents an example of a FOCSSY-type spectrum. A 2D  $J$ -resolved spectrum of the basic pancreatic trypsin inhibitor (BPTI) was measured. The sampling in this experiment started immediately after the  $180^\circ$  pulse (Fig. 1C). In Fig. 15A a section of this spectrum from  $\omega_2 = 4.19$  to 4.73 ppm is shown. The 1D spectrum extends along the diagonal because in contrast to the conventional echo-type  $J$ -resolved experiment (Fig. 1C') both chemical shift and coupling information is present during the evolution period  $t_1$  and the detection period  $t_2$ . The restricted  $\omega_1$  frequency range leads to multiple folding of the diagonal (Fig. 15A). With the foldover correction applied, the spectrum Fig. 15B results. Only six resonances between 4.25 and 4.45 ppm could not be properly relocated because their distance from the diagonal is larger than  $\pm\omega_N$ . In Fig. 15C the spectrum of Fig. 15B is presented after tilting (25). Figure 15D shows the same spectrum as Fig. 15C after symmetrization. In addition, the  $\omega_1$  frequencies were divided by two to remove the artifactual doubling of the frequency scale in the foldover correction calculation. This type of experiment has recently also been used by S. Macura and L. R. Brown (private communication).

## VII. PRESENTATION OF 2D PROTEIN SPECTRA

The enormous information content of 2D spectra of proteins necessitates a careful selection of the presentation of the data. In the past, stacked plot representations (Fig.

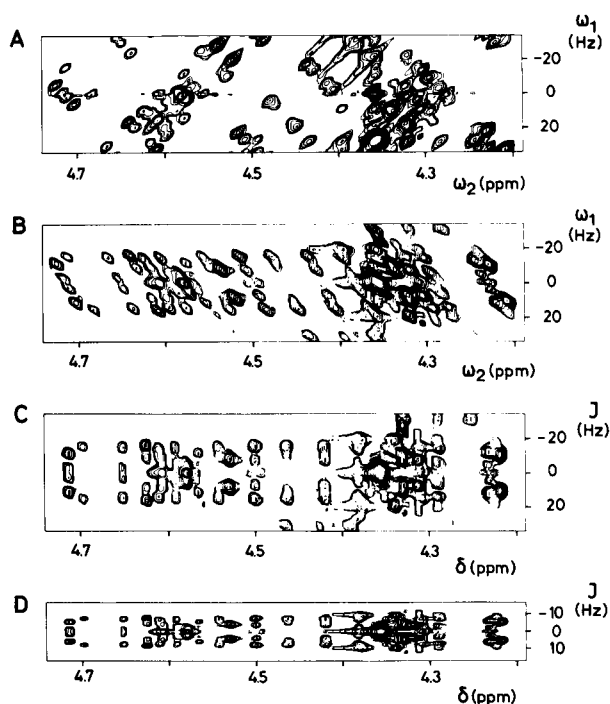


FIG. 15. Foldover-corrected spectroscopy (FOCSY). A 2D  $J$ -resolved spectrum recorded with the experiment of Fig. 1C in a 0.02  $M$  solution of the basic pancreatic trypsin inhibitor (BPTI) in  $^2\text{H}_2\text{O}$ ,  $T = 68^\circ$ ,  $\text{p}^2\text{H} = 4.7$  is shown. (A) Since the spectral width in the  $\omega_1$  direction is only 70 Hz, the spectrum is folded back many times. In this trace five fragments of the diagonal flanked by the multiplet components can be observed to rise at an angle of  $45^\circ$  relative to the  $\omega_2$  axis. (B) The same spectrum as in (A) after foldover correction; the data manipulation caused a doubling of the multiplet splittings. For six resonances between 4.25 ppm and 4.35 ppm the correction did not work because they have a larger distance from the diagonal than  $\pm\omega_N$  (see text). (C) Same spectrum as in (B) after tilting. (D) Same spectrum as in (C) after symmetrization and reduction of the  $\omega_1$  frequencies by a factor 2.

11) and contour plots (Figs. 3, 4, 9, 13, 15) have been employed to represent complete 2D spectra. Often, the relevant information is confined to selected cross sections (Figs. 12 and 14) and sometimes one-dimensional projections of the 2D spectra are useful means of representation (6, 25, 47).

#### (a) Stacked Plots

For obtaining a quick visual impression of a 2D spectrum, stacked plots are quite instructive although for a quantitative evaluation of the data they are usually useless. Stacked plots do not require much preprocessing of the data and can be obtained with any sufficiently fast XY recorder. Problems of resolution may arise when the number of lines to be drawn exceeds 256. The utility of stacked plots is thus confined to spectra with a limited number of spectral elements in the  $\omega_1$  domain, particularly to 2D  $J$ -resolved spectroscopy and to low-resolution SECSY plots. In some cases it is of advantage to suppress hidden lines, in other cases the information loss by this

cleanup procedure may be intolerable. Despite their disadvantages stacked plots are valid tools for "honest" representation of the original data. This contrasts somewhat to contour plots where essential features may often be hidden by an improper selection of contour levels.

*(b) Contour Plots*

For a quantitative evaluation of 2D spectra contour plots are invaluable. They are the most widely used representation of 2D data. The computation of the contours is a demanding task and requires a fair amount of computing time. Numerous procedures have been proposed in literature. The technique adopted in our software package uses a search procedure briefly described in Ref. (10).

The selection of the proper contour levels is of central importance for a pleasing and at the same time fair representation of the 2D data. It is recommended that for routine applications equidistant contour lines are selected. In special cases, a non-equidistant spacing may be applied. In all cases, the selected contour levels should clearly be stated in figure captions.

The representation of phase-sensitive spectra with positive and negative intensities is difficult in a contour plot and can most satisfactorily be solved by using a colour plot. For publications a representation of positive and negative intensities in two separate plots seems preferable. In reasonably well resolved spectra a superposition of broken contour lines representing negative peaks and solid contours depicting positive peaks may also be considered.

*(c) Cross Sections*

In many cases, selected cross sections contain all relevant information of 2D spectra (Figs. 12, 14). They should be used whenever accurate peak intensities or peak shapes must be represented (25, 47). They are also suitable in the case of very large dynamic ranges which are difficult to visualize in contour plots. In addition, negative signal intensities can be represented without problems in cross sections. Cross sections may become misleading when the resolution perpendicular to the cross section is insufficient and "cross-talk" between different cross sections cannot be avoided. Sometimes, it is useful to plot several adjacent sections through the same peak to visualize perpendicular tendencies.

*(d) Projections*

The utility of projections is limited to 2D  $J$ -resolved spectra where homonuclear broadband decoupled spectra can be obtained (6, 25, 47). They allow the "counting" of the individual protons and may be useful for the proper selection of the position of cross sections. Otherwise their utility in 2D protein NMR is somewhat limited.

## VIII. CONCLUSIONS

This paper attempted an account of practical procedures which have proved useful in two-dimensional spectroscopy of small proteins in solution. Two-dimensional spectroscopy has become an indispensable tool in our laboratory for the elucidation of

protein structure, which is also routinely used by biochemists and biophysicists without much previous knowledge of sophisticated NMR technology. Quite obviously, the procedures described are not exclusively applicable to proteins but would be equally well suited for the analysis of larger organic molecules in solution as well as for other biological macromolecules, such as nucleic acids (62).

We have limited this paper to the description of experimental procedures for the presently most widely used homonuclear 2D  $^1\text{H}$  NMR techniques in protein research. Many more techniques are known which are potentially of interest for the study of large molecules. We would like to mention relayed magnetization transfer for tracing out remote connectivities in spin systems (63, 64). Similar information can be obtained from multiple-quantum spectra (65, 66). For the simplification of overcrowded spectra, multiple-quantum filters (67, 68) and diagonal peak suppression procedures (69, 70) can be employed. Heteronuclear correlation experiments (71-75) also look promising for protein NMR despite inherent sensitivity problems. Most of these techniques involve similar experimental requirements as those discussed in this paper. Recent experience has also shown that absorption mode spectra can be considerably more informative than absolute value displays due to the narrower lineshapes and the resulting increased spectral resolution (7, 76-79).

For future work with proteins and other macromolecules the 2D NMR experiments will be selected from the techniques described in detail in this paper as well as from the more recently introduced measurements which are briefly mentioned in this last section. Various different considerations will influence the choice. These will include that relatively low-resolution, absolute-value spectra using similar parameters to those in Table 3 can be obtained with relatively short times for accumulation and data manipulation, whereas, for example, the recording of highly resolved phase-sensitive spectra is much more time consuming (78, 79). One may thus, for example, decide to forego resolution for efficient data accumulation in the early phases of a structure determination and complement this data at a later stage with highly resolved presentations of selected spectral regions. In view of the very large amounts of data obtained, for example, from a single NOESY spectrum of a protein, it can be foreseen that the use of computers for bookkeeping and for the structural analysis will be an important factor in future developments. This will undoubtedly also lead to new demands on the quality of the experimental 2D NMR spectra.

#### ACKNOWLEDGMENTS

Financial support by special grants of the Eidgenössische Technische Hochschule, Zurich, and by the Schweizerischer Nationalfonds (Project 3.528.79) are gratefully acknowledged. The authors are grateful to Dr. G. Bodenhausen and Dr. M. P. Williamson for helpful suggestions with regard to the manuscript, to Mr. A. Eugster for recording the spectra of Fig. 11, to Mrs. Y. Hunziker for drawing some of the figures and to Mrs. I. Kowalski (Spectrospin AG, Fallanden) for typing the manuscript. The authors also acknowledge the support by Spectrospin AG, Fallanden.

#### REFERENCES

1. K. NAGAYAMA, K. WÜTHRICH, P. BACHMANN, AND R. R. ERNST, *Biochem. Biophys. Res. Commun.* **78**, 99 (1977).
2. K. NAGAYAMA, K. WÜTHRICH, AND R. R. ERNST, *Biochem. Biophys. Res. Commun.* **90**, 305 (1979).
3. ANIL KUMAR, R. R. ERNST, AND K. WÜTHRICH, *Biochem. Biophys. Res. Commun.* **95**, 1 (1980).

4. O. JARDETZKY, "NMR and Biochemistry" (S. J. Opella and P. Lu, eds.), pp. 141-167, Decker, New York, 1979.
5. K. WÜTHRICH, K. NAGAYAMA, AND R. R. ERNST, *Trends Biochem. Sci.* **4**, N178 (1979).
6. W. P. AUE, J. KARHAN, AND R. R. ERNST, *J. Chem. Phys.* **64**, 4226 (1976).
7. W. P. AUE, E. BARTHOLDI, AND R. R. ERNST, *J. Chem. Phys.* **64**, 2229 (1976).
8. K. NAGAYAMA, ANIL KUMAR, K. WÜTHRICH, AND R. R. ERNST, *J. Magn. Reson.* **40**, 321 (1980).
9. A. BAX AND R. FREEMAN, *J. Magn. Reson.* **44**, 542 (1981).
10. J. JEENER, B. H. MEIER, P. BACHMANN, AND R. R. ERNST, *J. Chem. Phys.* **71**, 4546 (1979). 11. K. NAGAYAMA AND K. WÜTHRICH, *Eur. J. Biochem.* **114**, 365 (1981).
12. G. WAGNER, ANIL KUMAR, AND K. WÜTHRICH, *Eur. J. Biochem.* **114**, 375 (1981).
13. G. WAGNER AND K. WÜTHRICH, *J. Mol. Biol.* **155**, 347 (1982).
14. G. WIDER, K. H. LEE, AND K. WÜTHRICH, *J. Mol. Biol.* **155**, 367 (1982).
15. A. S. ARSENEV, G. WIDER, F. J. JOUBERT, AND K. WÜTHRICH, *J. Mol. Biol.* **159**, 323 (1982).
16. R. M. KELLER, R. BAUMANN, E. H. HUNZIKER-KWIK, F. J. JOUBERT, AND K. WÜTHRICH, *J. Mol. Biol.* **163**, 623 (1983).
17. R. V. HOSUR, G. WIDER, AND K. WÜTHRICH, *Eur. J. Biochem.* **130**, 497 (1983).
18. P. STROP, G. WIDER, AND K. WÜTHRICH, *J. Mol. Biol.* **166**, 641 (1983).
19. P. STROP, D. CECHOVA, AND K. WÜTHRICH, *J. Mol. Biol.* **166**, 669 (1983).
20. K. WÜTHRICH, G. WIDER, G. WAGNER, AND W. BRAUN, *J. Mol. Biol.* **155**, 311 (1982).
21. G. WAGNER AND K. WÜTHRICH, *J. Mol. Biol.* **160**, 343 (1982).
22. K. WÜTHRICH AND G. WAGNER, Ciba Foundation Symposium No. 93 on Mobility and Function in Proteins and Nucleic Acids, Pitman, London, 1983.
23. W. BRAUN, G. WIDER, K. H. LEE, AND K. WÜTHRICH, *J. Mol. Biol.* **169**, 921 (1983).
24. G. WAGNER, A. PARDI, AND K. WÜTHRICH, *J. Am. Chem. Soc.* **105**, 5948 (1983).
25. K. NAGAYAMA, P. BACHMANN, K. WÜTHRICH, AND R. R. ERNST, *J. Magn. Reson.* **28**, 29 (1978).
26. ANIL KUMAR, G. WAGNER, R. R. ERNST, AND K. WÜTHRICH, *Biochem. Biophys. Res. Commun.* **96**, 1156 (1980).
27. ANIL KUMAR, G. WAGNER, R. R. ERNST, AND K. WÜTHRICH, *J. Am. Chem. Soc.* **103**, 3654 (1981).
28. R. BAUMANN, ANIL KUMAR, R. R. ERNST, AND K. WÜTHRICH, *J. Magn. Reson.* **44**, 76 (1981).
29. R. BAUMANN, G. WIDER, R. R. ERNST, AND K. WÜTHRICH, *J. Magn. Reson.* **44**, 402 (1981).
30. S. MACURA, K. WÜTHRICH, AND R. R. ERNST, *J. Magn. Reson.* **46**, 269 (1982).
31. S. MACURA, K. WÜTHRICH, AND R. R. ERNST, *J. Magn. Reson.* **47**, 351 (1982).
32. G. WIDER, R. V. HOSUR, AND K. WÜTHRICH, *J. Magn. Reson.* **52**, 130 (1983).
33. R. V. HOSUR, R. R. ERNST, AND K. WÜTHRICH, *J. Magn. Reson.* **54**, 142 (1983).
34. R. FREEMAN AND G. A. MORRIS, *Bull. Magn. Reson.* **1**, 5 (1979).
35. A. BAX, "Two-Dimensional Nuclear Magnetic Resonance in Liquids," Reidel, London, 1982.
36. W. E. HULL, "Two-Dimensional NMR," Bruker, Karlsruhe, 1982.
37. M. BILLETER, W. BRAUN, AND K. WÜTHRICH, *J. Mol. Biol.* **155**, 321 (1982).
38. K. WÜTHRICH, *Biopolymers* **22**, 131 (1983).
39. M. BILLETER, Diploma Thesis, ETH-Zurich. Computerunterstützter graphischer Modellbau von Polypeptidketten unter Berücksichtigung von NMR-Daten, 1980.
40. W. BRAUN, C. BÖSCH, L. R. BROWN, N. GO, AND K. WÜTHRICH, *Biochim. Biophys. Acta* **667**, 377 (1981).
41. G. M. CRIPPEN AND T. F. HAVEL, *Acta Crystallogr. Sect. A* **34**, 282 (1978).
42. T. F. HAVEL, G. M. CRIPPEN, AND I. D. KUNTZ, *Biopolymers* **18**, 73 (1979).
43. K. Wüthrich, "NMR in Biological Research: Peptides and Proteins," North-Holland, Amsterdam, 1976.
44. K. NAGAYAMA AND K. WÜTHRICH, *Eur. J. Biochem.* **115**, 653 (1981).
45. K. NAGAYAMA, *Advan. Biophys.* **14**, 139 (1981).
46. G. KING AND P. E. WRIGHT, *Biochem. Biophys. Res. Commun.* **106**, 559 (1982).
47. G. WIDER, R. BAUMANN, K. NAGAYAMA, R. R. ERNST, AND K. WÜTHRICH, *J. Magn. Reson.* **42**, 73 (1981).
48. L. MÜLLER, *J. Magn. Reson.* **36**, 301 (1979).
49. D. I. HOULT AND R. E. RICHARDS, *Proc. Roy. Soc. London Ser. A* **344**, 311 (1975).
50. G. BODENHAUSEN, R. FREEMAN, AND D. L. TURNER, *J. Magn. Reson.* **24**, 511 (1977).

57. S. MACURA AND R. R. ERNST, *Mol. Phys.* **41**, 95 (1980).
52. S. MACURA, Y. HUANG, D. SUTER, AND R. R. ERNST, *J. Magn. Reson.* **43**, 259 (1981).
53. K. WÜTHRICH AND G. WAGNER, *J. Mol. Biol.* **130**, 1 (1979).
54. A. G. REDFIELD, S. D. KUNZ, AND E. K. RALPH, *J. Magn. Reson.* **19**, 116 (1975).
55. J. D. CUTNELL, *J. Am. Chem. Soc.* **104**, 362 (1982).
56. R. R. ERNST, *Advan. Magn. Reson.* **2**, 1 (1966).
57. J. C. LINDON AND A. G. FERRIGE, *Prog. NMR Spectrosc.* **14**, 27 (1980).
58. A. DE MARCO AND K. WÜTHRICH, *J. Magn. Reson.* **24**, 201 (1976).
59. A. BAX, A. F. MEHLKOPF, AND J. SMIDT, *J. Magn. Reson.* **35**, 373 (1979).
60. G. WAGNER, K. WÜTHRICH, AND H. TSCHESCHE, *Eur. J. Biochem.* **86**, 67 (1978).
61. E. BARTHOLDI AND R. R. ERNST, *J. Magn. Reson.* **11**, 9 (1973).
62. A. PARDI, R. WALKER, H. RAPOPORT, G. WIDER, AND K. WÜTHRICH, *J. Am. Chem. Soc.* **105**, 1652 (1983).
63. G. EICH, G. BODENHAUSEN, AND R. R. ERNST, *J. Am. Chem. Soc.* **104**, 3731 (1982).
64. G. WAGNER, *J. Magn. Reson.* **55**, 151 (1983).
65. L. BRAUNSCHEWEILER, G. BODENHAUSEN, AND R. R. ERNST, *Mol. Phys.* **48**, 535 (1983).
66. G. WAGNER AND E. R. P. ZUIDERWEG, *Biochem. Biophys. Res. Comm.* **113**, 854 (1983).
67. U. PIANTINI, O. W. SORENSEN, AND R. R. ERNST, *J. Am. Chem. Soc.* **104**, 6800 (1982).
68. T. H. MARECI AND R. FREEMAN, *J. Magn. Reson.* **51**, 531 (1983).
69. G. BODENHAUSEN AND R. R. ERNST, *Mol. Phys.* **47**, 319 (1982).
70. K. NAGAYAMA, Y. KOBAYASKI, AND Y. KYOGOKU, *J. Magn. Reson.* **51**, 84 (1983).
71. A. A. MAUDSLEY AND R. R. ERNST, *Chem. Phys. Lett.* **50**, 368 (1977).
72. A. A. MAUDSLEY, L. MÜLLER, AND R. R. ERNST, *J. Magn. Reson.* **28**, 463 (1977).
73. G. BODENHAUSEN AND R. FREEMAN, *J. Magn. Reson.* **28**, 471 (1977).
74. R. FREEMAN AND G. A. MORRIS, *J. Chem. Soc. Chem. Commun.*, 684 (1978).
75. T. M. CHAN AND J. L. MARKLEY, *J. Am. Chem. Soc.* **104**, 4010 (1982).
76. P. BACHMANN, W. P. AUE, L. MÜLLER, AND R. R. ERNST, *J. Magn. Reson.* **28**, 29 (1977).
77. D. J. STATES, R. A. HABERKORN, AND D. J. RUBEN, *J. Magn. Reson.* **48**, 286 (1982).
78. D. MARION AND K. WÜTHRICH, *Biochem. Biophys. Res Commun.* **113**, 967 (1983).
79. M. WILLIAMSON, D. MARION, AND K. WÜTHRICH, *J. Mol. Biol.*, submitted for publication.